Optimizing a Halbach cylinder for field homogeneity by remanence variation

Nielsen, Kaspar Kirstein; Insinga, Andrea Roberto; Bahl, Christian ; Bjørk, Rasmus

Published in:
Journal of Magnetism and Magnetic Materials

Link to article, DOI:
10.1016/j.jmmm.2020.167175

Publication date:
2020

Document Version
Peer reviewed version

Journal Pre-proofs

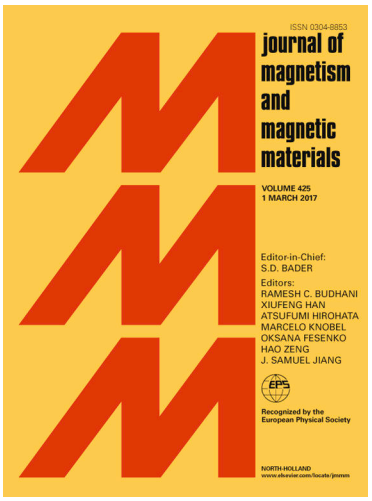

Optimizing a Halbach cylinder for field homogeneity by remanence variation

Kaspar K. Nielsen, Andrea R. Insinga, Christian R.H. Bahl, Rasmus Bjørk

PII: S0304-8853(20)30751-4
DOI: https://doi.org/10.1016/j.jmmm.2020.167175
Reference: MAGMA 167175

To appear in: *Journal of Magnetism and Magnetic Materials*

Received Date: 17 March 2020
Accepted Date: 21 June 2020

Please cite this article as: K.K. Nielsen, A.R. Insinga, C.R.H. Bahl, R. Bjørk, Optimizing a Halbach cylinder for field homogeneity by remanence variation, *Journal of Magnetism and Magnetic Materials* (2020), doi: https://doi.org/10.1016/j.jmmm.2020.167175

Optimizing a Halbach cylinder for field homogeneity by remanence variation

Kaspar K. Nielsen, Andrea R. Insinga, Christian R.H. Bahl and Rasmus Bjørk
kasparkn@gmail.com (corresponding author)
DTU Energy Conversion and Storage, Technical University of Denmark
Anker Engelundsvej Building 301
2800 Kgs. Lyngby, Denmark

June 23, 2020

Abstract

We investigate whether field homogeneity of a magnetic assembly can be optimized by varying the remanence of its constituting magnetic segments. We specifically study this hypothesis for a Halbach cylinder using a numerical model, MagTense. We consider a Halbach cylinder consisting of six layers of three concentric rings, each ring made from 16 segments. We show that ideally, the homogeneity can reach close to 1 ppm for a finite magnet.

We then proceed to consider a real world set of magnet segments, i.e. non-ideal magnets with a variation in their remanence. This reduces the field homogeneity to about 1000 ppm when considering a Gaussian perturbation of the remanence with a standard deviation of 1 %. However, we also show that the reduction in homogeneity may be countered by organizing the magnet pieces found through optimization, which is possible if each magnet segment is well characterized experimentally. We note that the presented method is applicable to any case where homogeneity of the field is important. The results we present are considered for the specific case of nuclear magnetic resonance for concretenes.

1 Introduction

Permanent magnet systems are relevant for numerous applications some of which require a large degree of field homogeneity. Examples include Nuclear Magnetic Resonance (NMR) [1] and Vibrating Sample Magnetometry [2]. Different design concepts of magnetic systems generating a highly homogeneous field have been investigated. Among these, the most notable are the C-shaped magnetic circuit [3] and the Halbach cylinder which is a hollow cylindrical shell segmented into several uniformly magnetized blocks. The Halbach cylinder [4] provides a very good compromise between size (weight and therefore cost), field strength and homogeneity.

Turek et al. provides a detailed analysis of segmented Halbach cylinders in terms of the field homogeneity in the bore as a function of sample size and number of segments [5]. This work clearly shows that a segmented finite Halbach cylinder is inherently limited in terms of the homogeneity it can produce. It is therefore necessary to modify the Halbach cylinder design for improving the field homogeneity if a Halbach cylinder is to be used as the base for applications demanding extremely high field homogeneity, such as NMR applications. An approach for solving this problem was presented in Ref. [6]. Here, the authors used a genetic algorithm for optimally placing permanent magnet pieces in a Halbach-like grid in order to improve the field homogeneity.

It is furthermore well-known that since a large magnet has to be build of individual pieces, or segments, there is a great potential for being sensitive to variations in the properties of the individual segments originating from manufacturing tolerances. Therefore, even though an optimal design balancing cost, sample size, field strength and homogeneity may be found by modifying a Halbach cylinder, variations in the actual individual magnet pieces may degrade the overall homogeneity.

In this paper we present an approach or algorithm for designing an optimal Halbach-like magnet that produces a field with given magnitude while maximizing the homogeneity. We incorporate the expected variation from manufacturing tolerances in the approach in a way that requires some detailed knowledge of the properties of the individual magnets physically acquired.

We perform this task by analyzing the field homogeneity of a finite and segmented Halbach-type [4] cylindrical magnet. The magnet configuration is build up by a number of rings stacked in the axial direction, where the rings consist of a number of concentric radial rings. Each of the rings comprises a Halbach magnet, as shown in Fig. 1. To explore different field strengths and geometries, we let the inner radius of the configuration and the sample region be fixed while the outer radius and the length of the magnet are varied, as only the relative geometrical parameters are important in magnetostatics. In this way, we find the field homogeneity at various field magnitudes as well as the amount of magnet material required, which directly relates to the cost and weight of the system.

For each configuration we vary the magnitude of the remanent magnetization of each segment through the use of an optimizer with the objective of improving the field homogeneity across the sample region. Then, in order to simulate actual manufactured permanent magnet blocks which have a tolerance on their magnetization, we assume each optimized configuration to be perturbed by a normal distribution applied to the remanent magnetization of each segment. This perturbation distorts the field and degrades the homogeneity.

We then exploit symmetry and the fact that, even though all the segments on the same radial ring have identical shape, when considering the magnetization direction each segment is present four times in each of our configurations. We apply an optimizer in order to remedy the distortion of the homogeneity by the normal distribution caused by the manufacturing tolerance. We do this by determining the optimal position of the segments within the Halbach cylinder structure. One may view this

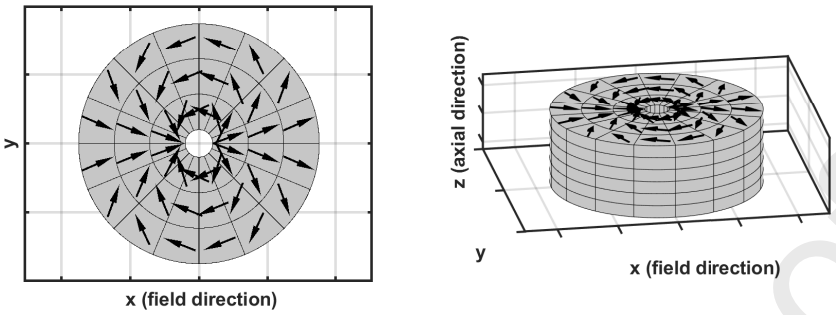

(a) (b)

Figure 1: The segmented magnet configuration seen in the xy-plane (a) and in perspective (b). Note the three radial rings in the six axial layers consisting of 16 segments each. The black arrows show the magnetization direction for a Halbach cylinder.

as having bought the exact (nominal) segments required for a given design, then meticuously characterizing them individually and subsequently placing them as optimally as possible, thus restoring some of the field homogeneity from the initial optimal design.

2 Model

The magnet model, known as MagTense [7], is based on three-dimensional geometrical units (tiles) within which the magnetization is assumed homogeneous. In the present work we consider one type of tile: a piece of a hollow cylinder defined by its angular extent ($\delta\phi$), radial extent (δr) and thickness in the axial direction (δz); see Fig. 2. The center of the tile is positioned in cylindrical coordinates at r_0, ϕ_0 and z_0. Assuming the tile to be homogeneously magnetized with magnetization vector $\mathbf{M}_0$, the magnetic induction $\mathbf{B}$ or equivalently magnetic field $\mathbf{H}$ may be found at any point inside or outside the tile through the demagnetization tensor field, $\mathbb{N}$. A tile centered at $\mathbf{r}'$ will generate a magnetic field, $\mathbf{H}$, at a location in space $\mathbf{r}$ given by the demagnetization tensor field $\mathbb{N}$:

$$\mathbf{H}(\mathbf{r}) = \mathbb{N}(\mathbf{r} - \mathbf{r}') \cdot \mathbf{M}(\mathbf{r}'), \tag{1}$$

where the tile is assumed to be homogeneously magnetized. The derivation of the tensor field, $\mathbb{N}$, is given in Ref. [8].

In order to find the magnetization within a given tile, it is necessary to find the magnetic field inside the tile and subsequently apply a constitutive relation valid for the present magnet material. We find the field at a given point $\mathbf{r}$ as the superposition of the fields from all n tiles in the model:

$$\mathbf{H}(\mathbf{r}) = \sum_{i=1}^{n} \mathbf{H}_i(\mathbf{r}). \tag{2}$$

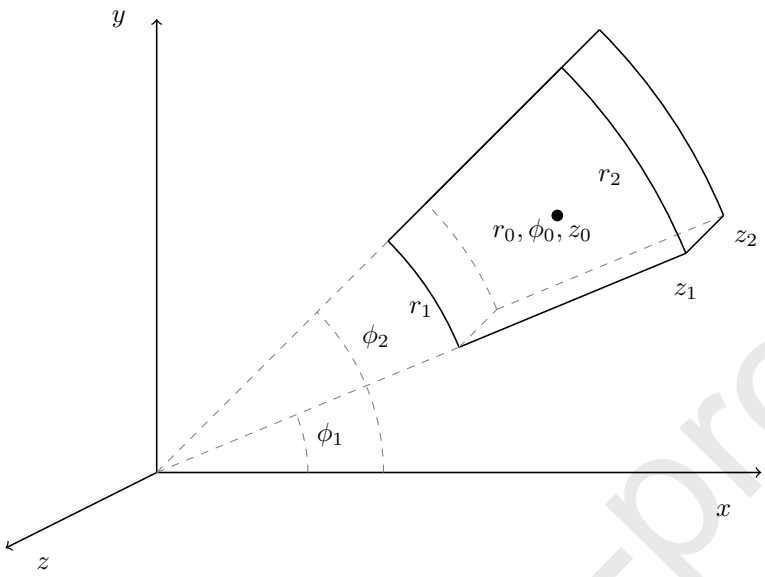

Figure 2: The cylindrical tile on which each magnet segment is based. Note that $r_0 = \frac{1}{2}(r_1 + r_2)$, $\phi_0 = \frac{1}{2}(\phi_1 + \phi_2)$ and $z_0 = \frac{1}{2}(z_1 + z_2)$ while $\delta r = r_2 - r_1$, $\delta\phi = \phi_2 - \phi_1$ and $\delta z = z_2 - z_1$.

Given the local field in a tile we assume the following constitutive relation for the permanent magnet material:

$$\mathbf{M} = (\boldsymbol{\mu}_r - I)\mathbf{H} + \mathbf{M}_{\text{rem}}. \tag{3}$$

Here I denotes the identity matrix and $\boldsymbol{\mu}_r$ the anisotropic relative permeability tensor, which is given by

$$\boldsymbol{\mu}_r = P \begin{pmatrix} 1.06 & 0 & 0 \\ 0 & 1.17 & 0 \\ 0 & 0 & 1.17 \end{pmatrix} P^{-1}, \tag{4}$$

where P is the change of basis matrix from the local coordinate system (V_i') of the given tile to the global Cartesian coordinate system (V). The latter coordinate system is defined in the conventional way with Origin at the center of the magnet and the axial direction of the magnet parallel to the $z-$direction. The former coordinate systems are defined individually for each tile such that the first axis is parallel to the easy axis $\mathbf{u}_{\text{ea}}$ of the given magnet segment, the second axis $\mathbf{u}_{\text{ha1}}$ is simultaneously perpendicular to $\mathbf{u}_{\text{ea}}$ and to the third axis $\mathbf{u}_{\text{ha2}}$, which is parallel to the z-axis of the global system. The first and second axes of the local coordinate systems are thus mutually orthogonal and lie in the same plan as the global $x-$ and $y-$axes and are thus rotated with respect to these. This change of basis is necessary, as the relative permeability is different along the easy axis, compared to the perpendicular directions, simply because

of the anisotropy of NdFeB magnets [9]. The values of the relative permeability tensor are assumed constant, i.e. they do not depend explicitly on the field, and thus only small changes in the magnetization vector are allowed.

The easy axis of each tile and thus the tile's local coordinate system is defined through the Halbach [4] formula for a dipole Halbach magnet with the field in the center bore. This is given in Cartesian coordinates as:

$$[\mathbf{u}_{\mathrm{ea}}]_V = (\cos 2\phi, \sin 2\phi, 0)^\top, \tag{5}$$

with ϕ being the conventional azimuthal angle about the z-axis measured counterclockwise from the x-axis. The transformation from the local coordinate system V' to the global Cartesian coordinate system V is performed by the matrix P having as columns the global coordinates of the easy vector shown in Eq. 5 along with the previously defined two hard axis unit vectors:

$$P(\phi) = \{[\mathbf{u}_{\mathrm{ea}}]_V; [\mathbf{u}_{\mathrm{ha1}}]_V; [\mathbf{u}_{\mathrm{ha2}}]_V\} \tag{6}$$

$$= \begin{pmatrix} \cos 2\phi & -\sin 2\phi & 0 \\ \sin 2\phi & \cos 2\phi & 0 \\ 0 & 0 & 1 \end{pmatrix}. \tag{7}$$

It is noted that P is an orthogonal matrix and thus $P^{-1} = P^\top$.

The remanent magnetization is assumed to be parallel to the easy axis and may thus be written in the global coordinate system as

$$\mathbf{M}_{\mathrm{rem}} = M_0 \left[\mathbf{u}_{\mathrm{ea}}\right]_V, \tag{8}$$

with M_0 denoting the nominal remanence of the magnet material at zero field.

The magnetic flux density $\mathbf{B}$ at a point $\mathbf{r}$ from a tile is found, as mentioned above, by assuming said tile to be homogeneously magnetized and free currents to be absent. Through the vector potential formulation it is possible to find $\mathbf{B}$:

$$\begin{aligned} \mathbf{B} &= \boldsymbol{\nabla} \times \mathbf{A} \\ \mathbf{A}(\mathbf{r}) &= \frac{\mu_0}{4\pi} \int_S \frac{\mathbf{M}(\mathbf{r}') \times \hat{\mathbf{n}}(\mathbf{r}')}{|\mathbf{r} - \mathbf{r}'|} \mathrm{d}a'. \end{aligned} \tag{9}$$

Here, the normal vector to the closed surface S with area element $\mathrm{d}a'$ is denoted $\hat{\mathbf{n}}$ and is explicitly a function of the primed coordinates, which denote in turn the coordinates on the surface that is integrated over. The vacuum permeability is μ_0. The details about the evaluation of the integral in Eq. 9 are given in full in Ref. [8].

Finally, we state the defining equation for the magnetic field:

$$\mathbf{H} = \frac{1}{\mu_0}\mathbf{B} - \mathbf{M}. \tag{10}$$

2.1 Self-consistent model solution

For a given problem a number of tiles are configured following the cylindrical Halbach design. Equation 1 is then solved together with Eq. 2 in order to find the field **H** within each tile. Equation 3 is subsequently applied in order to update the magnetization. This iteration is continued until the relative change in the magnetization in each tile is less than a pre-specified tolerance, here set to 1e−10.

The geometrical part of the model, i.e. solving Eq. 1 needs only to be done once for a given configuration due to the assumption of a homogeneous magnetization within each tile. This can be formulated as a sum of tensor products as in Eq. 2:

$$\mathbf{H}(\mathbf{r}) = \sum_{i=1}^{n} \mathbf{H}_i(\mathbf{r}) = \sum_{i=1}^{n} P\left(\mathbb{N}(P^{-1}\left(\mathbf{r}-\mathbf{r}'\right)) \cdot P^{-1}\mathbf{M}(\mathbf{r}')\right), \tag{11}$$

where $\mathbb{N}$ denotes the demagnetization tensor field that captures the geometrical part of the problem. It is noted that the tensor field calculation takes approximately 1 minute on a single Intel Xeon CPU running at 3.6 GHz. Once this calculation has been done and the tensor field is found for the whole problem, one may use Eq. 11 directly in the iterative scheme and the total model solution time on the same system becomes about 0.3 s. This enables a significant amount of model runs to be done in a reasonable amount of time given a fixed geometry while varying the remanence of the segments. It is noted that $\mathbb{N}$ is found in the local coordinate system of the given tile.

The analytical expression of the geometrical demagnetization tensor, and the iterative approach to compute self-consistent solutions have been validated against results obtained by means of numerical simulations. The simulations have been performed with the finite element analysis software COMSOL Multiphysics. These comparisons show excellent agreement between the solutions obtained with the two approaches [8] thus validating the approach used here.

2.2 Optimization algorithm

In this paper, the basic hypotheses are that

- The field homogeneity of a segmented magnet configuration may be optimized by varying the remanence of the segments among the values corresponding to different magnet grades.
- Real magnet segments that are nominally identical come with a statistical spread in their remanence both in terms of magnitude and direction. These deviations will negatively influence the field homogeneity due to asymmetry in the system. However, this effect may be partially remedied by optimizing the placement of individual segments that are nominally identical within the magnet configuration.

Both hypotheses require an optimization scheme in order to be evaluated. As the geometry is kept fixed, we are addressing a combinatorial optimization problem. Therefore, we have chosen to use the genetic algorithm (GA) as this method has been proved to handle discrete problems

Table 1: The remanence of the commercially available NdFeB magnet grades. The list is taken from Bakker Magnetics [10]. Similar values are claimed by other magnet vendors.

Grade	N28UH	N30UH	N33UH	N35UH	N38UH	N40UH	N42UH	N44SH
Remanence [T]	1.08	1.12	1.17	1.22	1.26	1.30	1.33	1.36

effectively [6]. The optimization objective is to minimize the peak-to-peak value of the field inside a spherical region with a radius of 2 mm centered at the center of the magnet. The peak-to-peak (p2p) value is defined conservatively as:

$$\text{p2p} \equiv \frac{\max(H) - \min(H)}{\max(H)}, \tag{12}$$

where the max and min operators are evaluated with respect to the position over a spherical volume with radius 2 mm centered in the bore of the magnet as stated above and H is the magnetic field norm. Clearly, when the field is perfectly homogeneous within the spherical volume, the value of p2p goes to zero.

The optimization algorithm is split into two parts, corresponding to the two basic hypotheses presented above, respectively. In the *first part* the magnitude of the magnetization of each segment is allowed to vary according to a pre-defined set of allowed (discrete) values corresponding to the standard NdFeB magnet grades listed in Table 1. High coercivity UH and SH grades were chosen to avoid any issues of self-demagnetisation in the assemblies. Since eight-fold symmetry in the Halbach configuration is assumed only 1/8 of the number of segments are considered as variables for the GA.

Once a locally optimal configuration of remanence magnitudes has been found in this way, a perturbation is applied in order to model real-world magnets that come with a statistical spread in their magnetization relative to the nominal value. In this paper, we only consider variation in the magnitude of the remanence, but it is highly probable that a variation in the direction is also present. This choice is meant for simplicity and clarity; the algorithm works just as well on orientational variation. The off the shelf variation in the remanence of a specific grade is in general around 4 % for most magnet vendors. This is a combination of directional and magnitude variation. Upon request it is possible to obtain more homogeneous series of magnets within a specific grade. Thus, we here assume a variation in the remanence given by a Gaussian distribution with a standard deviation of 1 %.

The *second part* of the optimization algorithm has the goal of mitigating the effects of the Gaussian perturbation. For this purpose, we apply a slightly different optimization strategy. It is now assumed that all n segments have been characterized sufficiently accurately that the 1 % variation is well resolved. Each segment in our configuration can be placed in four different positions due to symmetry. In this way, the optimizer considers a number of groups, n_{g} of nominally identical segments where $n_{\text{g}} = n/4$. Within each group, the four perturbed segments can be

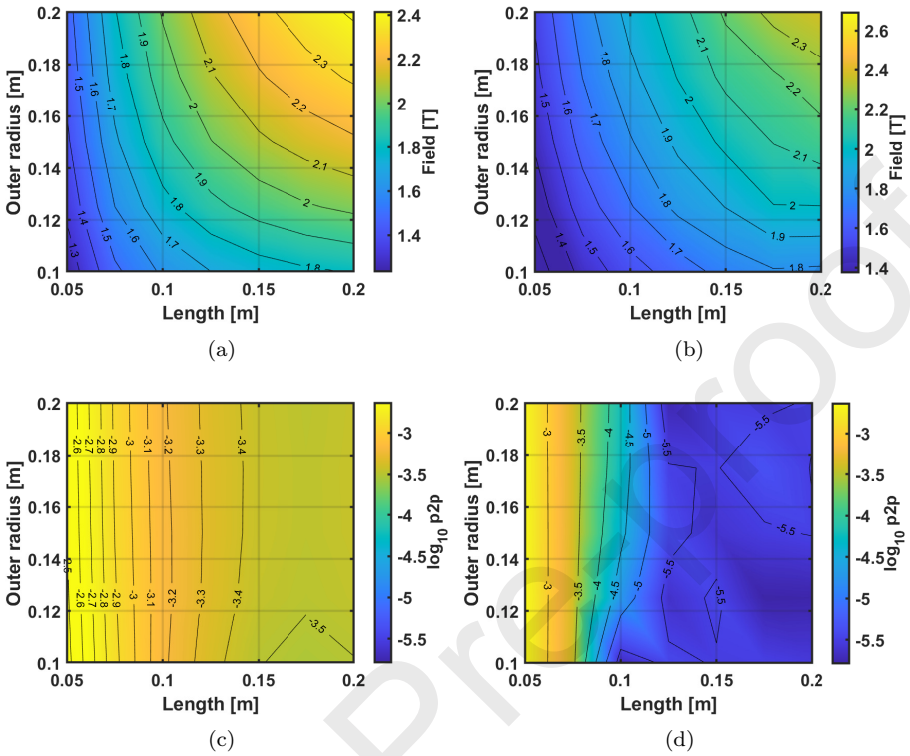

Figure 3: The average magnetic field and $\log_{10}$ p2p values as a function of length and outer radius for the nominal Halbach configuration ((a) and (c)) and for the optimized configuration ((b) and (d)), respectively.

placed at any position thus creating $4! = 24$ permutations for each group. In order to input this into the GA, we use a lexicographical indexing algorithm [11] and thus have a number of variables equal to the number of groups where each variable is an integer varying between 1 and 24.

3 Results and discussion

In the following we will consider a case of three concentric Halbach magnet rings each having 16 segments equally spaced in the azimuthal direction and consisting of six layers in the axial direction, as also shown in Fig. 1. This choice was made in order to have a geometry with room for variability and keeping symmetry. With this configuration we have thus a total of 288 magnet segments which are grouped into 72 groups each with four identical magnets.

We let the length, L and the outer radius, R_o vary between 0.05 and 0.2 m and 0.1 and 0.2 m, respectively, while keeping the radius of the bore, R_B fixed at 40 mm. Note that only the relative geometrical properties are

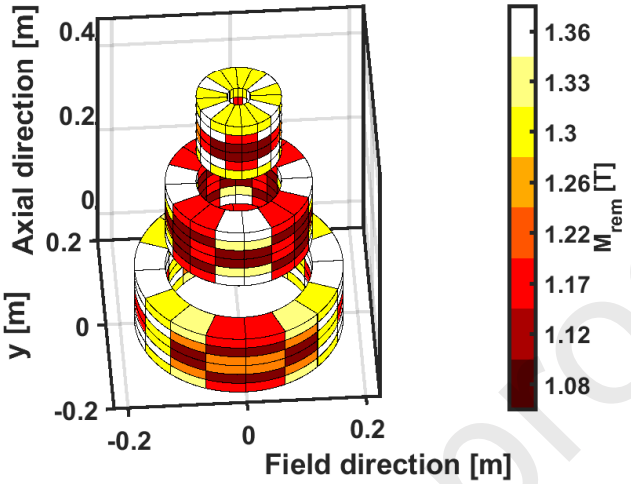

Figure 4: Exploded view of a locally optimal solution for the longest magnet configuration with $R_o = 0.1$ m. The colors indicate the resulting remanence of the magnet segments (note the 8-fold symmetry).

of importance.

3.1 Optimal placement of standard NdFeB grades

For comparison, we start with the basic configuration where all the magnet segments have the same nominal remanence of 1.22 T (the center of the list in Table 1). The resulting average magnitude of the field in the sample region is shown in Fig. 3(a). The corresponding field homogeneity, denoted p2p, is shown in Fig. 3(c) and it is observed that i) the homogeneity improves as a function of length and ii) it is greater than 300 ppm in all cases. The diminishing end effects of the longer magnet improve the field homogeneity, however modestly.

To improve the homogeneity, we then apply our first optimization strategy and let the remanence of each segment (exploiting 8-fold symmetry) vary between the discrete values given in Table 1. The resulting field and p2p homogeneity of the optimized configurations are given in Figs. 3(b) and 3(d), respectively. The produced field decreases between 0.1 and 0.3 T while the p2p values increase by up to two orders of magnitude, thus bringing the field homogeneity down to a few ppm.

The optimized configuration for a specific case is shown in the exploded plot in Fig. 4. As can be seen from the figure, it is hard to determine the logic behind the ordering of the individual magnet segments. However, a trend is that segments near the ends of the cylinder generally have a larger remanence than segments closer to the center. This most likely happens to limit flux leakage through the ends of the cylinder.

3.2 Perturbing the optimized solution

Having found a locally optimal configuration employing the approach discussed above, one may consider the choice of which magnets to obtain settled. Upon reception of these magnets from a magnet producer one might then perform some measurement in order to verify the magnets' properties and subsequently label each magnet individually with its actual magnetization. It is clear that even a small variation across the magnets will cause the magnet configuration to be asymmetric and thus make the field considerably less homogeneous.

To model this situation, we perturb the remanence of the individual blocks of the solutions presented in Fig. 3(d) with a normal distribution with a standard deviation of 1 %, as discussed above. The perturbation was applied through 50 different permutations of the same single normal distribution composed of 288 random values, i.e. one for each magnet segment. Doing this we obtain the results shown in Figs. 5(a) and 5(c) for the mean p2p and minimum p2p values, respectively. It is seen that the field homogeneity decreases with about two orders of magnitude due to the statistical variation, interesting enough bringing us back to about the same level of field homogeneity as before the optimal remanence was determined.

3.3 Re-optimizing the perturbed solutions

We then test our second hypothesis, i.e. that placing the actual magnet segments in a locally optimal way may partially remedy the decrease in homogeneity. For each of the 50 permutations we re-optimized the positioning of the magnet pieces while considering the 288 pieces to be distributed in 72 groups of four each yielding 24^{72} possible permutations. We found through running the GA optimizer on this using the lexicographical indexing as mentioned above that between 10,000 and 20,000 model runs were sufficient to find a local optimum. The results for the mean and minimum p2p values are given in Figs. 5(b) and 5(d), respectively. A gain between a half and one order of magnitude is achieved through this method.

3.4 Probability of getting a satisfying configuration

As the perturbation and re-optimization scheme discussed above is inherently statistical, it is instructive to consider certain probabilities. Given the ability to measure and characterize the deviation of a specific magnet segment from its nominal behavior one may ask with what probability will a certain batch of magnet segments be possible to arrange in such a way as to yield a field homogeneity better than a certain value?

To answer this question, we first consider the histogram in Fig. 6, which shows how the perturbed and re-optimized solutions of a certain geometric configuration behave statistically. It is clear that the re-optimization does not guarantee a better homogeneity than the perturbed system. However, it is also clear that there is a finite probability that re-arranging

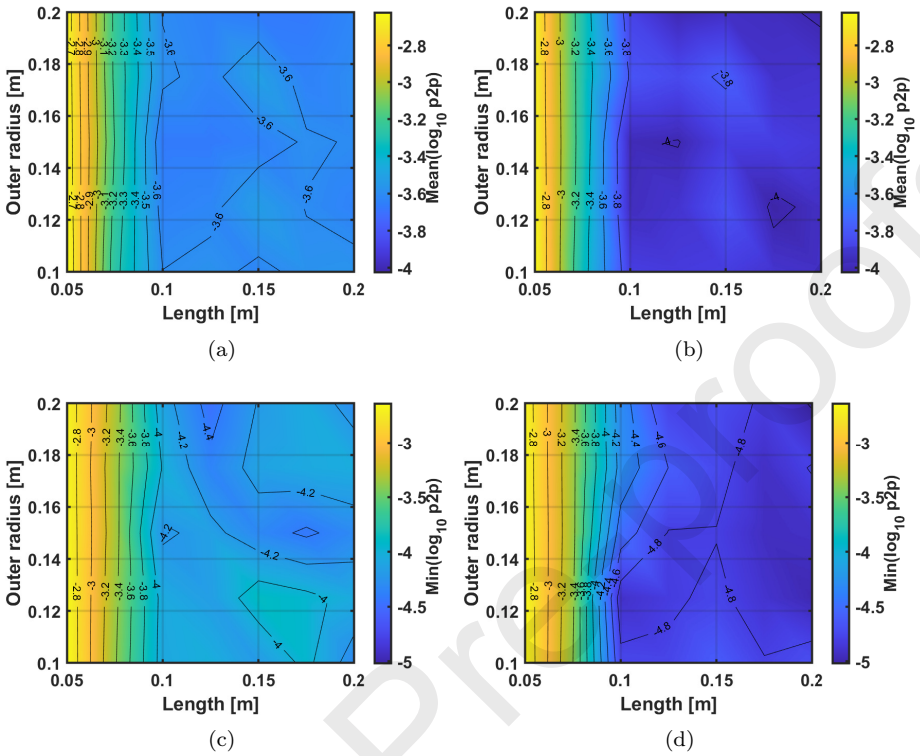

Figure 5: The mean of $\log_{10}$ p2p as a function of length and outer radius for the perturbed (a) and re-optimized (b) systems and the corresponding minimum values of $\log_{10}$ p2p for the perturbed (c) and re-optimized (d) systems.

the magnet segments in a clever way may actually increase the field homogeneity significantly.

The histogram in Fig. 6(a) shows the distribution of the perturbed and re-optimized solutions for the 1 % standard deviation perturbation while Fig. 6(b) shows the corresponding histogram for a perturbation with 5 % standard deviation (closer to off the shelf value). In the latter case, the perturbed solutions distribute roughly similar to those in the former case. However, the re-optimized solutions form a very narrow distribution around $\log_{10}$ p2p $= -3.27$ thus indicating that for too large a standard deviation, it is not feasible to find a way to organize the magnet segments such that an improved configuration may be obtained.

The results for all configurations of the Halbach cylinder are shown in Fig. 7, which shows the probability of obtaining a solution with a p2p value less than 100 ppm ($\log_{10}$ p2p < -4) for the perturbed case 7(a) and for the re-optimized case 7(b). Again, when the magnet is 0.1 m or longer the homogeneity increases and it is clear that the re-optimized systems have a significantly larger probability of yielding a p2p value better than

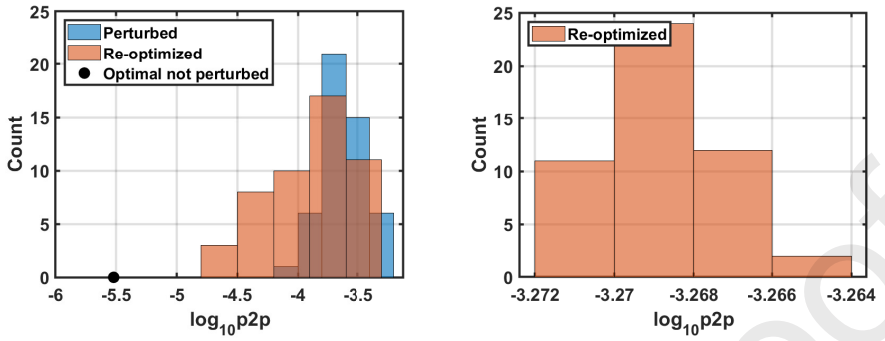

(a) (b)

Figure 6: (a) Histogram for the number of perturbed and re-optimized cases for the Halbach configuration with $L = 0.15$ m and $R_{\text{out}} = 0.1$ m given a 1 % standard deviation of the perturbed magnets. The black dot shows the pre-perturbed optimized configuration. (b) The resulting histogram when re-optimizing a 5 % standard deviation perturbation. Please note the highly compressed scale of the abscissa as compared to the figure in (a).

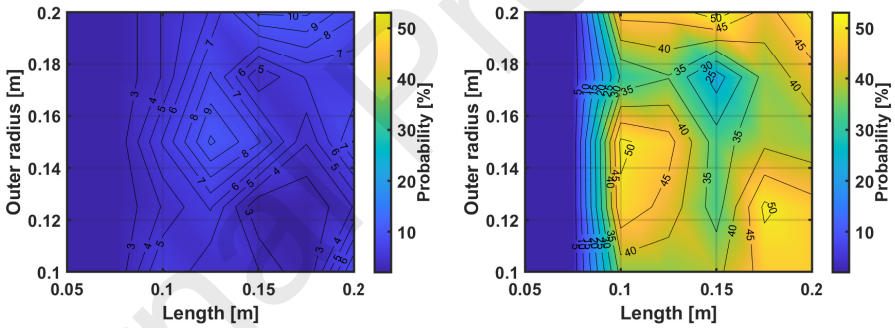

(a) (b)

Figure 7: The probability of obtaining a configuration with $\log_{10} < -4$ for the perturbed case (a) and the re-optimized case (b), respectively.

100 ppm than the perturbed systems have.

4 Conclusions

Because of statistical deviations from the nominal remanence, buying off the shelf permanent magnet segments will degrade the expected homogeneity of a given configuration. We hypothesized that this detrimental effect may be partially countered by placing nominally identical segments locally optimally. This hypothesis was proven to be right in the sense

that we clearly show that the probability of obtaining a solution with a smaller p2p value is larger when the magnet segments are arranged in a clever way found through optimization.

Our algorithm natively supports directional variation of the magnetization as well and essentially any magnet configuration desired. Nonetheless, we chose to focus on a single, yet relevant example for clarity. Future work would definitely explore the influence of directional variation and analyze other basic magnet configurations.

Finally, it should also be noted that one might consider buying a number of identical sets of magnet segments in the hope that one of them, after careful characterization, can be assembled to yield a desired p2p value. In our discussion of probabilities one might say that there is a 50 % change of achieving 100 ppm or better when buying one set of magnets. With two sets this increases to 75 % and five sets it is 97 %. Having so many segments one might cross-link them into multiple configurations, e.g. with two sets there would be eight magnets for each group of four positions. Solving this problem through an optimizer will require significantly more computational time, however, it does seem realistic to do in the not so far future. It is also noted that for perturbations with standard deviation larger than 1 % it is increasingly difficult or not feasible to find an optimized solution.

Acknowledgements

K.K. Nielsen wishes to thank the Danish Research Council for Independent Research — Technology and Production Sciences for support (contract no. 7017-00034) for financial support.

Rasmus Bjørk wishes to thank the Energy Technology Development and Demonstration Program (EUDP) under the Danish Energy Agency, project no. 64016-0058 for partly financial support of this work.

References

[1] I. I. Rabi, J. R. Zacharias, S. Millman, and P. Kusch. A new method of measuring nuclear magnetic moment. *Physical Review*, 53(4):318–318, 1938.

[2] S FONER. Versatile and sensitive vibrating-sample magnetometer. *Review of Scientific Instruments*, 30(7):548–557, 1959.

[3] Rongsheng Lu, Hong Yi, Weiping Wu, and Zhonghua Ni. Development of a miniature permanent magnetic circuit for nuclear magnetic resonance chip. *Chinese Journal of Mechanical Engineering (english Edition)*, 26(4):689–694, 2013.

[4] K. Halbach. Design of permanent multipole magnets with oriented rare earth cobalt material. *Nuclear Instruments and Methods*, 169(1):1–10, 1980.

[5] Krzysztof Turek and Piotr Liszkowski. Magnetic field homogeneity perturbations in finite halbach dipole magnets. *Journal of Magnetic Resonance*, 238:52–62, 2014.

[6] Clarissa Zimmerman Cooley, Melissa W. Haskell, Stephen F. Cauley, Charlotte Sappo, Cristen D. Lapierre, Christopher G. Ha, Jason P. Stockmann, and Lawrence L. Wald. Design of sparse halbach magnet arrays for portable mri using a genetic algorithm. *Ieee Transactions on Magnetics*, 54(1):A2224, 2017.

[7] R. Bjørk and K. K. Nielsen. MagTense. Technical University of Denmark, DTU Energy, Department of Energy Conversion and Storage. `https://doi.org/10.11581/DTU:00000071`, 2019.

[8] Nielsen K.K and Bjørk R. The demagnetization tensor for a homogeneously magnetized cylindrical tile. *J. Magn. Magn. Mater.*, Submitted, 2019.

[9] M. Katter. Angular dependence of the demagnetization stability of sintered nd-fe-b magnets. *Intermag Asia 2005. Digests of the Ieee International Magnetics Conference, 2005*, pages 945,946, 945–946, 2005.

[10] Bakker magnetics standard grades. `https://bakkermagnetics.com/wp-content/uploads/2019/01/neodymium_sintered_-_standard_grades_0.pdf`.

[11] Private communication with Mr. Eric Oullet. `https://www.codeproject.com/Articles/1250925/Permutations-Fast-implementations-and-a-new-indexi`.